Geological, geochemical and mineralogical characteristics of the Bamhantara bauxite over Deccan Basalt Province of Kabirdham district, Chhattisgarh, India

Debjani Sarkar[1,*], Pradipta Sur[2] and Dinesh Kumar Thawait[3]

[1]Geological Survey of India, State Unit: West Bengal and Andaman, Bhu-Bijnan Bhavan, DK-6, Sector-II, Salt Lake, Kolkata 700 091, India
[2]Geological Survey of India, Eastern Region, Bhu-Bijnan Bhavan, DK-6, Sector-II, Salt Lake, Kolkata 700 091, India
[3]Geological Survey of India, Kanchanganga Colony, Amanaka, Raipur 492 010, India

This study presents the probable environment from petrographical, mineralogical and geochemical analyses of representative samples from Bamhantara block, Kabirdham district, Chhattisgarh, India using EPMA and SEM-EDS for petrological study, and XRF and ICP-MS for geochemical inference. Microscopic study revealed the dominance of boehmite minerals that specify the syn-environmental depositional condition, while circular/well-rounded pisolitic texture indicated autochthonous deposits. The geochemical study determined the progressive changes in major, trace and REE concentrations from precursor rock to bauxite during weathering. Bamhantara bauxite has been formed under oxidizing (positive Ce anomalies; Ce/Ce*, 0.92–2.15) and near alkaline to alkaline ($(La/Yb)_N$ and La/Y ratio > 1) conditions. The analogous trend of REE for bauxite/laterite and precursor rock indicates that lateritic bauxite had an autochthonous origin and is a chemical disintegration product of Deccan Trap basalt under tropical to subtropical climates. The geochemical behaviour of REE revealed that bauxite/laterite was generated from type-2 basalt characterized by positive Ce, Eu and Dy anomaly. The low concentration of kaolinite indicates desilication under a hot tropical climate.

Keywords: Bauxite, basalt, laterite, precursor rock, weathering.

LATERITES and bauxite deposits form duricrusts during intense tropical weathering conditions[1]. The world's largest bauxite deposits are mainly distributed in tropical and subtropical regions on both sides of the equator between latitudes 30°S and 30°N (ref. 2). Major bauxite mining occurs in northern South America, West Africa, India, Southeast Asia, and northern to southwestern Australia[3]. Generally, three types of bauxitic minerals are found, viz. gibbsite ($Al_2O_3 \cdot 3H_2O$), boehmite (AlO(OH)) and diaspore; whereas laterite is a mixture of varying proportions of goethite (FeO(OH)), hematite (Fe_2O_3), limonite (γ-FeO(OH)) and kaolinite ($Al_2Si_2O_5(OH)_4$) (refs 4–6). The large gibbsite deposits are located in Guyana Shield, Guinea, Australia, Brazil and India[7,8]. There are mainly two types of bauxite deposits – laterite-type bauxite formed from the weathering of igneous, metamorphic or sedimentary rocks, and karst bauxite formed in limestone terrain[9]. In India, the existence of extensive belts of laterite along the Maikal range hills is well-documented. This laterite-type bauxite developed over the Deccan continental flood basalt province[10]. During the Cenozoic period, the multi-phase rift history of India played an important role in the morpho-tectonic evolution and the associated erosional, depositional and deep weathering of the massive basaltic province[11]. It might have contributed to the development of laterite and bauxite. The weathering profiles also played an important role in the evolution of tropical and subtropical landscapes of India, Africa and Australia[12–15]. Generally, laterite developed from ultramafic rocks due to strong weathering depending upon the climatic and topographical conditions[16,17]. Factors such as the type of protoliths, pH variation during weathering, adsorption processes, groundwater geochemistry, variation of Fe concentration in the weathering profiles, leaching degree of minerals and geochemistry of elements have played an important role in the distribution of elements during weathering. Bauxite/laterite is formed by intense chemical weathering of rocks under warm and humid climates, leading to the accumulation of least soluble metals and transportation of soluble elements[18–23]. Water percolation through the faulted and fractured parent rocks was extremely efficient in leaching silicates and concentration of aluminium in the form of bauxite[24]. The development and destruction of the lateritic horizon depend solely on long-term climatic and tectonic stability along with slow geomorphological evolution over 10^4–10^6 years (ref. 25). Two of the most important environmental parameters are precipitation and temperature. Other factors such as vegetation[26,27], role of bacteria[28], role of groundwater[29,30], effect of the alternation of dry and wet seasons[26], and effect of topography[26,31] are also important to the lateralization process. That process was terminated by the upliftment, climate changes or both, and

*For correspondence. (e-mail: debjanisarkar.geology@gmail.com)

led to the rapid erosion and stripping of the lateritic weathering profile.

The highly elevated bauxite deposits within Fe-duricrusted surfaces (above 900 m) in the Bamhantara area of Kabirdham district, Chhattisgarh, India, were formed from the successive weathering of the Deccan Volcanic Province. The formation of bauxite is the result of a combination of geomorphological, groundwater regime and leaching factors[32]. It has been reported that bauxite in this area occurs in the form of pockets sandwiched between two highly ferruginous laterite horizons[33–35]. Further exploration was done during the last four decades due to the inaccessibility and logistic problems of this remotely situated top part of the plateau. The mineable bauxite resource was first discovered in the study area. The Bamhantara plateau has been estimated to contain 5 million tonnes of bauxite deposit in a total prospecting lease (PL) area of 0.78 km^2. The deposit has been studied in detail by other researchers[36–38]. The present study focuses on the analysis of detailed geological and mineralogical characteristics of bauxite deposits of the Bamhantara plateau in Kabirdham district, Chhattisgarh, to determine the concentration of major, trace and rare earth element (REE) in the bauxite ores developed within laterite over the Deccan Traps. The results of this study provide an opportunity to interpret the geo-environmental behaviour of bauxite formation in the Bamhantara plateau and similar types of deposits with similar geological set-ups elsewhere in the world.

Geological setting

The Bamhantara plateau is covered by laterite capping over the Deccan flood basalt province. Deccan basalt is fine-grained, light greenish-grey coloured, vesicular and amygdaloidal[39] at an altitude ranging from 340 to 941 m amsl, formed at the central part of the Maikal Hills of the Satpuras in Kabirdham district, Chhattisgarh (Figure 1). Today, the province has gained global attention because of its enormous volume and basaltic eruption duration that overlapped the Cretaceous–Tertiary boundary[10,40,41]. Samples collected from the Bamhantara plateau are covered by 0–5 m thick nodular and pisolitic lateritic soil. Some laterites have indurated surfaces or sandy textures, while others have a massive structure with colours ranging from brick red to dark brown (Figure 2 *a*). The bauxite horizon found below the top lateritic soil is hard, compact, pinkish-white to white in colour, massive and pisolitic at some places (Figure 2 *b* and *c*). In a few parts, the bauxite horizons bifurcate to form two separate layers. The concentration of ferruginous material in laterite increases below the bauxite horizon. It overlies the Deccan basalts through the intermediate zone of lithomargic clay with a gradational contact (Figure 2 *d*). Bauxite occurs more or less as horizontal lenses, lenticular patches, and tabular bodies in the form of boulders in pockets enclosed within[42]. The primary features have resulted from residual weathering leading to the formation of lithomargic clay, bauxite and laterite[43]. Figure 3 shows the subsurface disposition of lateritic soil, bauxite, ferruginous bauxite and clay horizons in the Fence diagram. The depth of the ore zone varied from 0 to 7.63 m. Supplementary Table 1 summarizes the cumulative thickness of bauxite in 133 boreholes.

Materials and methods

In recent years, various analytical techniques have been used to determine major, trace and REE geochemistry and to study the parent rock composition, diagenetic and epigenetic processes and environmental conditions (Eh–pH, drainage and climate). Field investigation of the Bamhantara block was carried out by detailed mapping (scale – 1 : 2000) and exploration (UNFC: G1 and G2 stage). A total of 194 boreholes were drilled at 50 m × 50 m intervals in an area of 1 km^2. A total of 558 samples were used for the analysis from at least 148 boreholes. The core samples (558) were

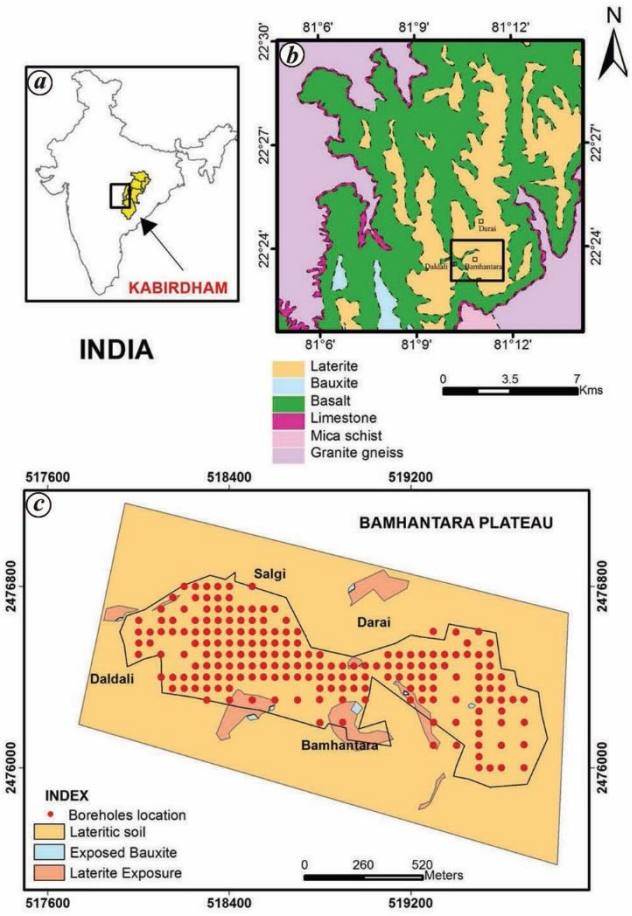

Figure 1. ***a***, Location map of Kabirdham district, Chhattisgarh, India. ***b***, Geological map (part) of T.S. no. 64F/3. ***c***, Geological map (scale 1 : 2000) of Bamhantara area, Kabirdham district and borehole locations in the study area.

collected and analysed (selected major oxides: SiO_2, Al_2O_3, Fe_2O_3, TiO_2, loss of ignition (LOI)) from 148 boreholes. Among these, 133 boreholes were found to be productive in terms of bauxite after chemical analysis (Supplementary Table 1). In addition, 16 representative samples from the outcrops and also from the selected boreholes, six samples from basalt, one sample from saprolite outcrop, six samples from bauxite and three samples from laterite were collected for whole-rock geochemical analysis (all major oxides like SiO_2, Al_2O_3, Fe_2O_3, TiO_2, MgO, MnO, CaO, Na_2O, K_2O and minor elements like Ba, Mb, Sr, Zr, Y, Rb, REE) (Supplementary Table 2). Similarly, ten borehole samples were studied for mineralogical and textural analysis using ore microscopy followed by electron probe microanalyzer (EPMA) and scanning electron microscopy coupled with energy-dispersive X-ray spectrometry (SEM-EDS).

The standard methodology of X-ray fluorescence (XRF) and inductively coupled plasma-mass spectrometry (ICP-MS) techniques for chemical analysis was adopted for this study[44–48].

The major oxides, as well as trace elements and REEs were analysed by XRF and ICP-MS respectively, in the Geological Survey of India (GSI), Central Region, Nagpur, Maharashtra and State Directorate of Geology and Mining (DGM), Raipur, Chhattisgarh. LOI content was obtained by measuring the weight loss of 1 g of the sample after 90 min of heating at 950°C. The samples were processed for the whole-rock mineralogical composition of ores. All the representative samples were pulverized to obtain homogeneous samples. Approximately 1–2 kg of each sample was ground to finer size using agate jars and agate milling balls and sieved to ~120 mesh size.

Mineralogy at the microscale was studied by EPMA. For the study of bauxite ore, silicates, oxides and pure elements were used as standards (analytical errors was 1% for major elements and 3% for minor elements)[49]. Prior to analysis, the samples were typically coated with a thin film of conducting material (carbon) of about 20 nm thick for better conductivity. During EPMA, the samples were loaded only in the sample chamber through a vacuum interlock and mounted on the sample holders. Thin sections were studied using a polarizing microscope (Nikon) in Optical Microscope Laboratory of GSI, Central Region, Nagpur, Maharashtra. After a detailed petrographic analysis, the samples were studied using transmitted, and backscattered electron (BSE) images obtained when the electron beam was rastered on the sample. The brightness of individual

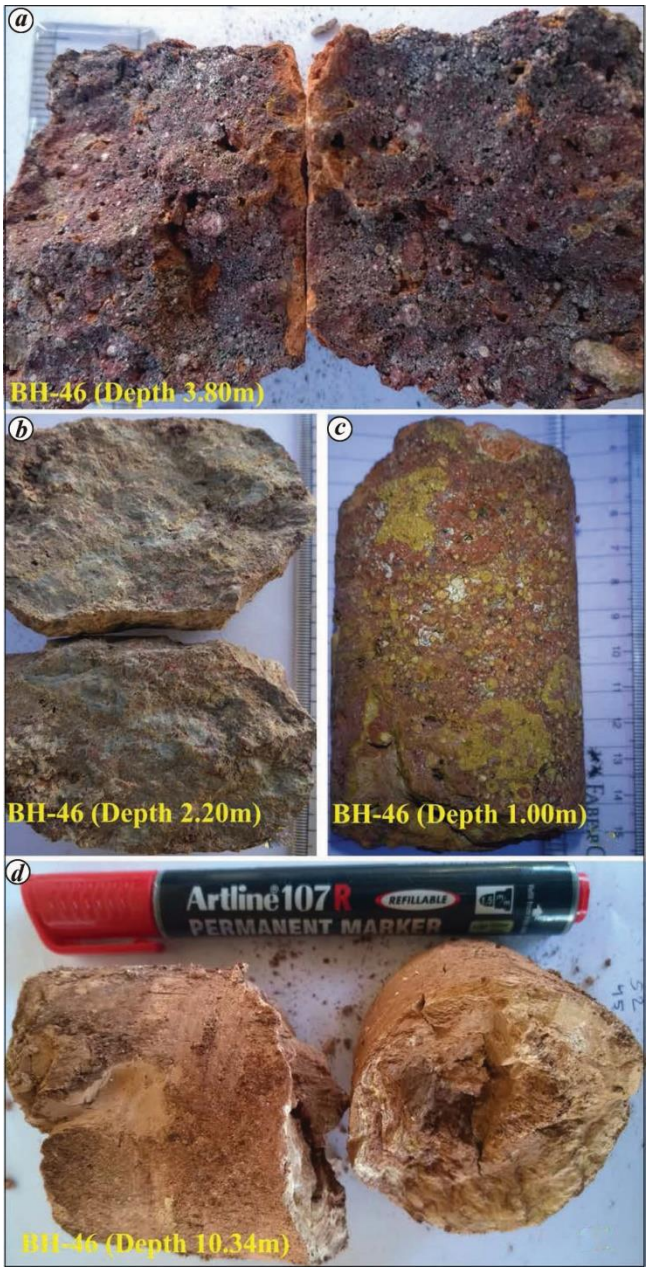

Figure 2. Photographs of core sample. ***a***, Brick-red-colours ferruginous laterite (BH no. 46); ***b***, pinkish-white to greyish-white massive bauxite (BH no. 46); ***c***, pinkish pissolitic bauxite (BH no. 46); ***d***, greyish massive lithomargic clay.

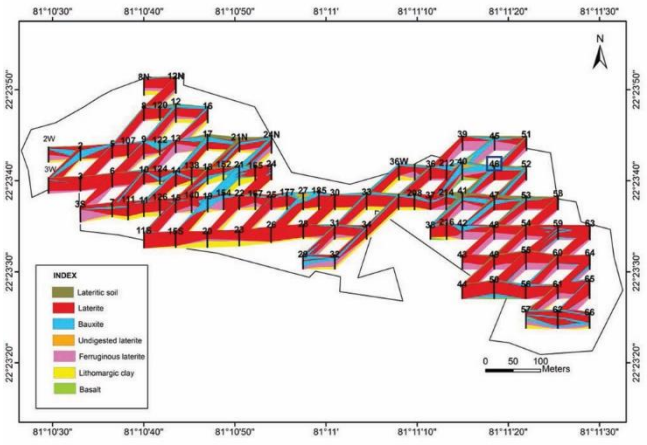

Figure 3. Fence diagram showing subsurface disposition of bauxite, ferruginous bauxite, laterite and lithomargic clay of Bamhantara area, Kabirdham district, Chhattisgarh.

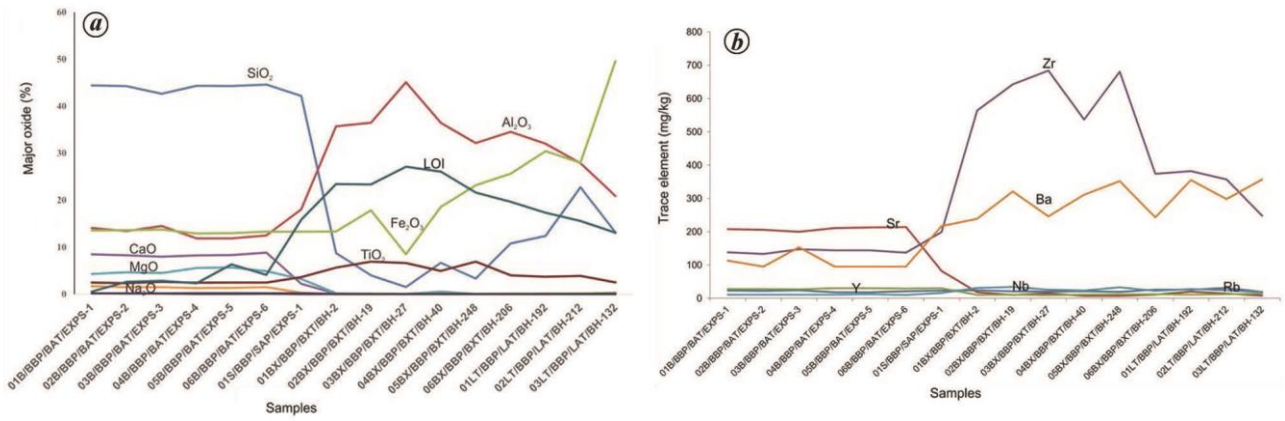

Figure 4. Changes in (***a***) major oxides (%) concentration from precursor rock to bauxite; (***b***) trace elements (mg/kg) concentration with weathering.

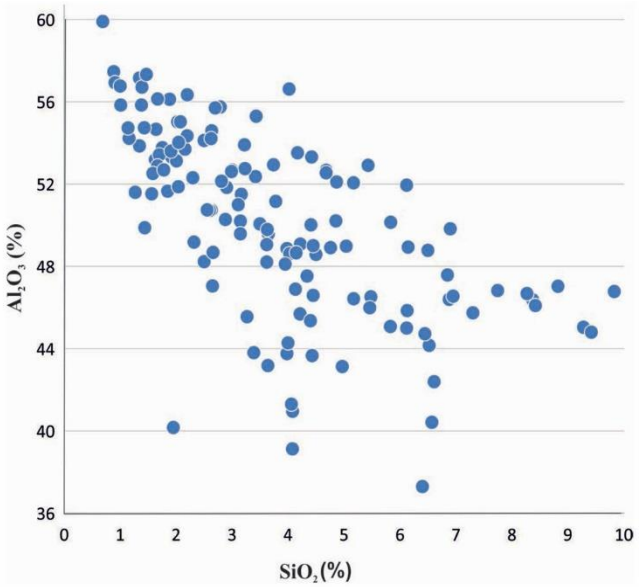

Figure 5. Distribution of SiO_2 (%) with respect to Al_2O_3 (%) for bauxite/laterite samples collected from 148 boreholes.

phases in the images is based on the average atomic number of the phases present in the sample and helps us understand the compositional variations between the mineral phases or within a single phase. The optical image, BSE image and chemical composition of minerals in thin sections were compared to explore the interaction of a mineral with a high energy (20 kv) electron beam focused to a diameter of a few microns[50].

Results

The analysis of major elements concentration revealed that SiO_2 abruptly decreases with progressive weathering from basalt to laterite with a sharp neck point at the saprolitic zone (Figure 4 *a*). The average silica percentage gradually decreases from basalt to bauxite: 44.11 in basalt, 42.17 in saprolite, 16.10 in laterite and 5.84 in bauxite (Supplementary Table 2). Quartz is not found in bauxite. The mean trace elements concentration of Zr, Ba and Nb increases 2–4 times from the parent rock to the bauxite/laterite profile, whereas the average concentration of Y and Sr decreases 2–20 times from basalt to bauxite. Rb concentration remains constant throughout the weathering process (Supplementary Table 2 and Figure 4 *b*).

The SiO_2 versus Al_2O_3 plot in Figure 5 also reveals that quartz is negligible with increased Al_2O_3 content in bauxite.

The petrological and mineralogical characteristics of bauxite indicate that mainly two types of bauxite are present in the study area, viz. massive (Figure 6 *a* and *b*) and oolitic–pisolitic (Figure 7 *a*–*d*). In the massive bauxite, aggregates of fine- to medium-grained gibbsite are frequently transacted by alumino-ferruginous material (Figure 6 *a*). The needle-shaped ilmenite occurs in a criss-cross pattern (Figure 6 *b*). The pisolitic bauxite shows oolitic–pisolitic, nodular texture under the microscope, with ooids of various shapes and sizes (Figure 7 *a*–*d*). The pisolites are mostly circular to elliptical in nature. The spherical grains of pisolites range from 400 to 800 µm. In elliptical grains, the long axis varies from 47 to 133 µm and the short axis from 43 to 118 µm. Gibbsite and boehmite occurred in the core of pisolites and are surrounded by the alumino-ferruginous, cryptocrystalline (often microcrystalline) brown-coloured, Fe–Ti-rich clay matrix (Figure 7 *a*, *c* and *d*). These have been considered ilmenite grains within hematite and goethite. Although the matrix is heterogeneous, spotted and ferruginous in composition tiny veinlets and voids are occupied by boehmite (Figure 7 *a* and *d*). The aggregates of boehmite form concentric bands at a few places (Figure 7 *b*, *c* and *d*). The Ti and Fe concentration increases from core to rim (Figure 7 *b*). Goethite is present along the boundary of pisolites. The aggregates of fine- to medium-grained gibbsite are frequently transacted by the alumino-ferruginous material. The gibbsite–boehmite transitional phase was observed in the thin-section analysis at a few selected parts of the study area (BH no. 64) (Figure 8 *a*). The colloform bands

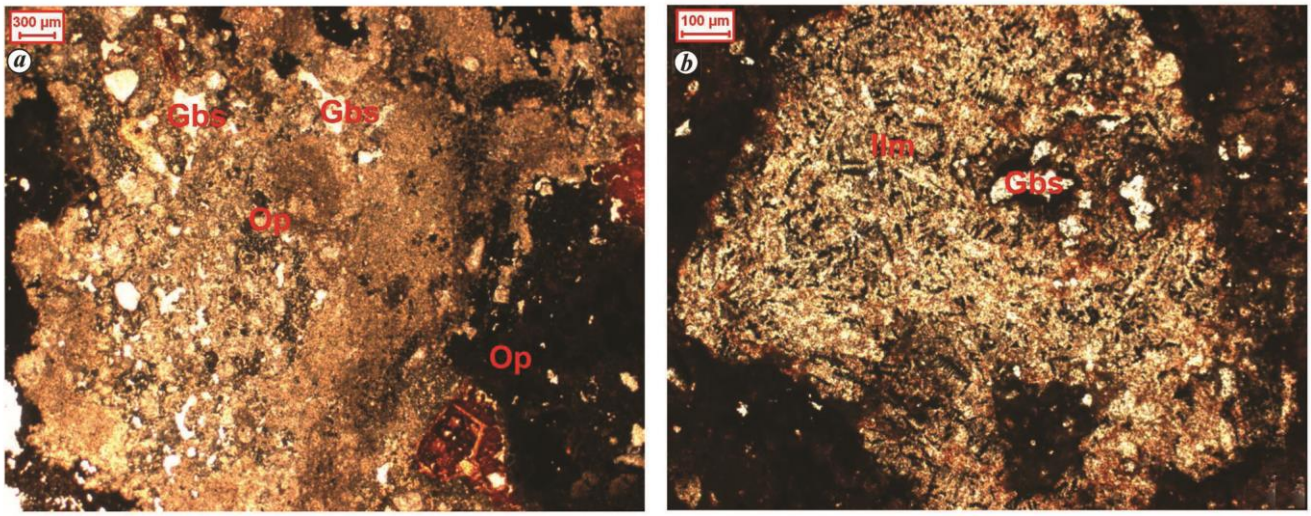

Figure 6. Photomicrographs of (***a***) massive bauxite (BH-14) with small specks of opaque minerals (plane polarized light, PPL); (***b***) massive fine crystalline bauxite with small specks of ilmenite (Ilm*) minerals (BH-52) (PPL)[94].

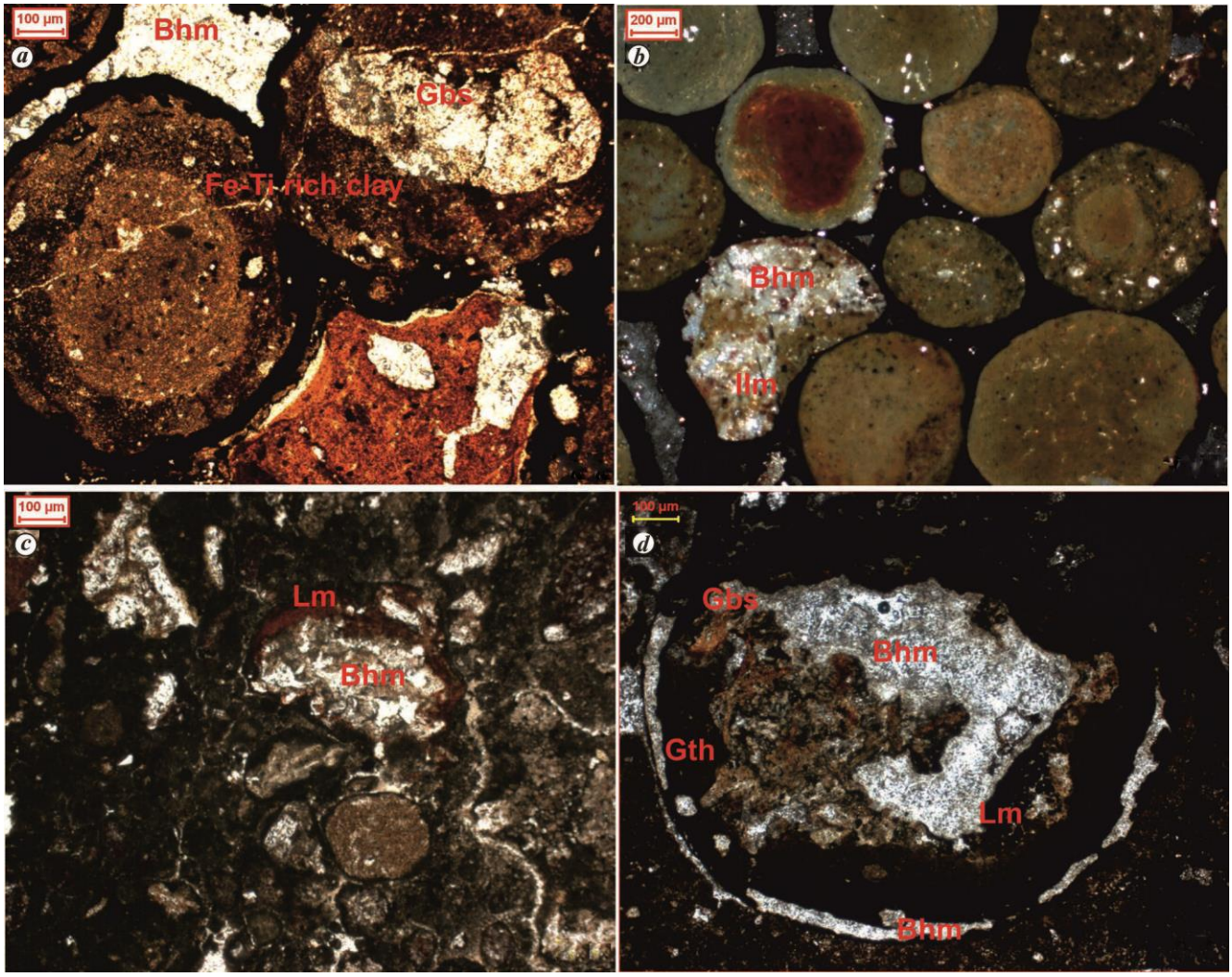

Figure 7. Photomicrographs showing the texture and mineralogy of bauxite occurring in the study area. ***a***, Pisolitic bauxite (BH-14). The centre is formed by gibbsite (Gbs*) and surrounded by Fe–Ti-rich clay along with goethite (Gth*) (PPL). ***b***, Pisolitic bauxite (BH-64). The core is formed by boehmite (Bhm*) (PPL). ***c***, Fine pisolitic bauxite (BH-3W). The core is composed by boehmite (Bhm*) encircled by limonite (Lm*) (PPL). ***d***, Pisolitic bauxite with the central part showing boehmite (Bhm*) surrounded by limonite (Lm*) and gibbsite (Gbs*) (PPL)[94].

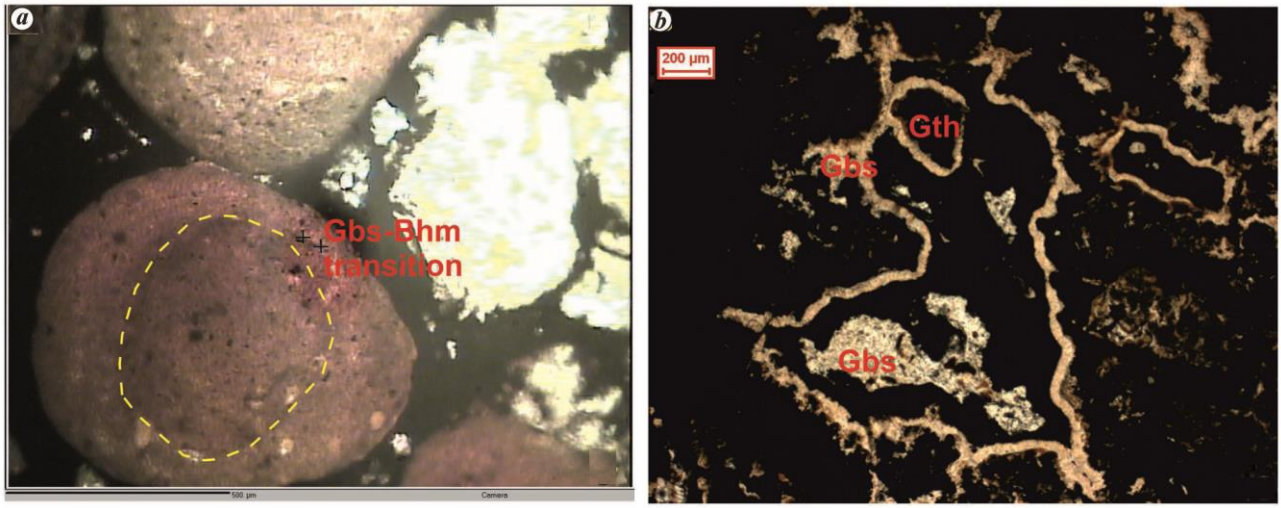

Figure 8. Photomicrographs of (***a***) colloform banding and rimmed texture formed by gibbsite (Gbs*) and opaque (Op*) (BH-47) (PPL) and (***b***) gibbsite and boehmite (Gbs*–Bhm*) transitional phase with low (5.72%) to moderately high (15%) amounts of TiO_2. Chemical changes observed within the oolites from core to boundary are indicated by the colour variations. Al_2O_3 content increases and FeO content decreases from core to boundary (BH no. 64)[94].

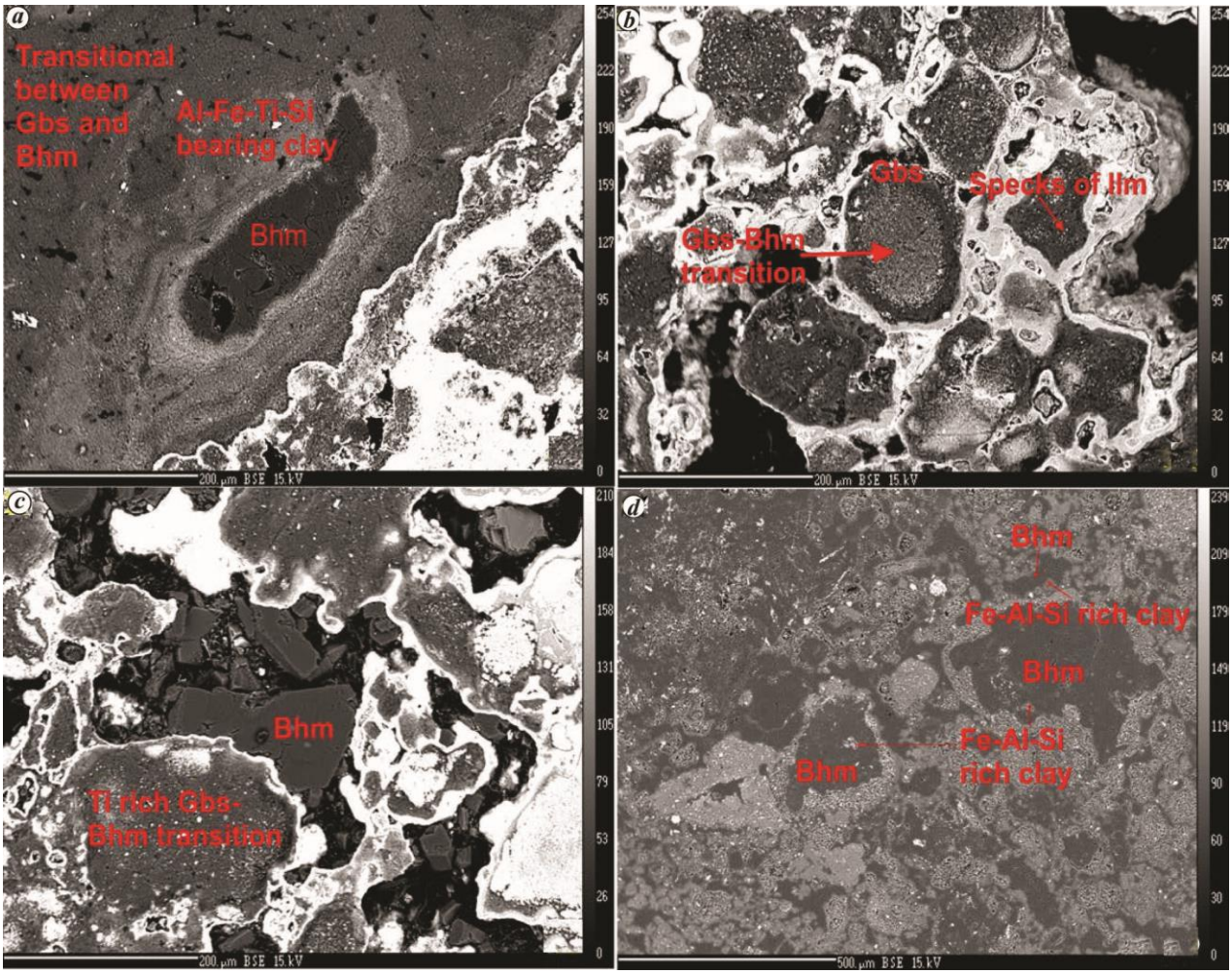

Figure 9. Backscatter electron (BSE) images: ***a***, Boehmite (Bhm*) encircled by Al–Fe–Ti–Si-bearing clay. Gibbsite (Gbs*)–boehmite (Bhm*) transitional phase and goethite are also present (BH-14). ***b***, Pisolitic bauxite, with the core formed by gibbsite (Gbs*)–boehmite (Bhm*) transitional phase encircled by gibbsite (Gbs*). Specks of ilmenite (Ilm*) are also present within bauxite (BH-47). ***c***, Ti-rich gibbsite (Gbs*)–boehmite (Bhm*) transition and boehmite (Bhm*) (BH-47). ***d***, Boehmite (Bhm*) along with Fe–Al–Si-rich clay (BH-36W).

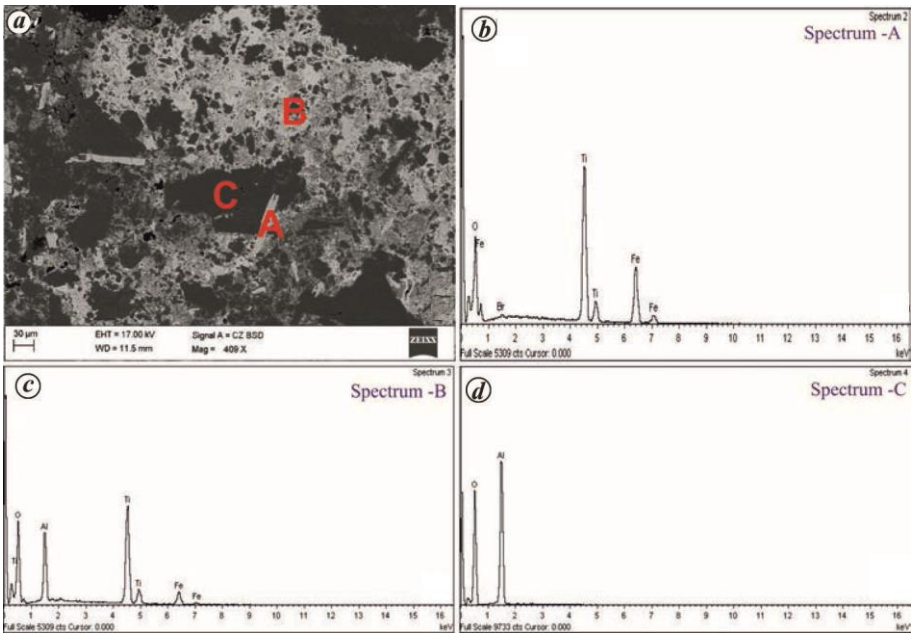

Figure 10. BSE images of bauxite ores of BH 46. Spectrum A shows needle-shaped ilmenite grain crosscuting the grain boundary of bauxite (spectrum C). Both the grains, i.e. ilmenite and bauxite are embedded within a matrix (spectrum B) that is mainly composed of 31.47 wt% Ti, 51.42 wt% O, 7.87 wt% Fe and 9.25 wt% Al.

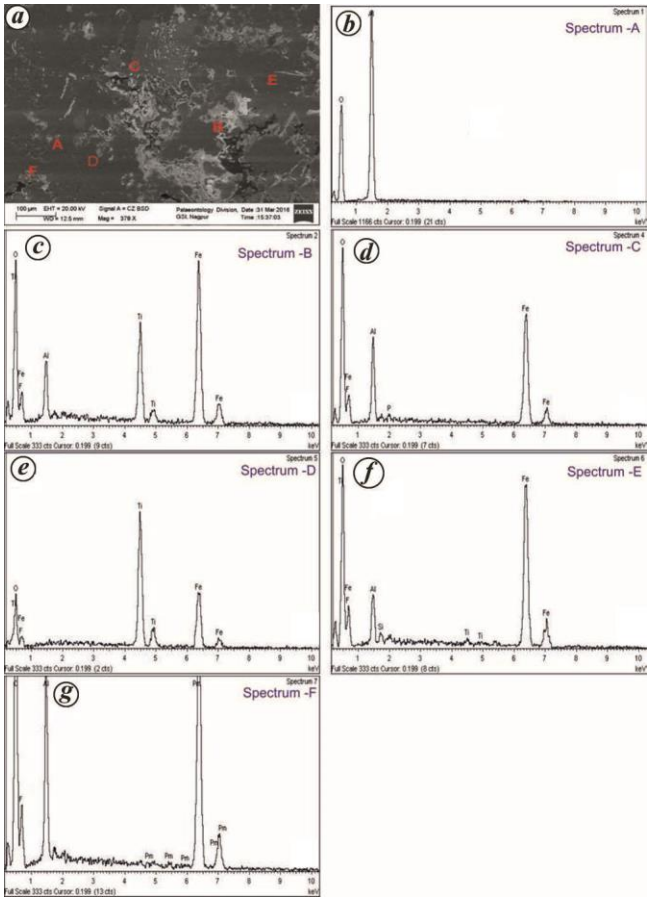

Figure 11. BSE images of bauxite ores of BH 117. Spectra A and B indicate pure bauxite and Ti–Fe-rich bauxite respectively. Within Fe-rich bauxite (spectrum C), trails of ilmenite (spectrum D) can be seen. Spectrum E shows Ti–Fe-rich bauxite, while spectrum F shows Promethium (REE).

formed alternating coloured rings of gibbsite and goethite/limonite (Figure 8 *b*). Negligible amount of kaolinite was observed in the bauxite samples. In general, hematite, goethite and kaolinite are the early minerals, and gibbsite is the late mineral for the formation of bauxite[51].

The detailed mineralogical study of bauxite samples by EPMA indicated that boehmite was the predominant aluminous mineral of the study area rather than gibbsite (Figure 9 *a*–*d*). The criss-cross arranged ilmenite grains were observed prominently by SEM-EDS (Figures 10 and 11). Sometimes the needle-shaped ilmenite grains showed triangular to polygonal interspace filled by bauxite (Figure 12).

The ternary plot of Al_2O_3–Fe_2O_3–LOI of bauxite samples of the study area showed that most of them occupied the boehmite/diaspore window[52] (Figure 13). The triangular variation diagrams of Al_2O_3–SiO_2–Fe_2O_3 are commonly used to show the degree of lateritization, mineral control and bauxite classification[53,54]. Based on the mineralogical classification, most of the bauxite samples in the study area fell within the ferrite bauxite and bauxite fields (Figure 14 *a*). The trivariate diagram of SiO_2–Al_2O_3–Fe_2O_3 in Figure 14 *b* indicates different degrees of lateritization and attests to the formation of the ore under intense lateritization conditions[54].

REEs are important to recognize bauxitization history. Minor amount of HREE, i.e. Pm (8.08 wt%), was determined during SEM-EDS (Figure 11). The light REE (∑LREE; La–Eu), heavy REE (∑HREE; Tb–Lu), and ∑REE (La–Lu) concentrations in the Bamhantara bauxite ranged from 59.16 to 91.13 mg/kg (average 73.72 mg/kg), 3.83 to 9.83 mg/kg (average 5.73 mg/kg) and 65.39 to 100.96 mg/kg (average 79.45 mg/kg) respectively (Supplementary Table 2). The

REE concentration in the Deccan basalt varied from 89.00 to 165.86 mg/kg (average 112.61 mg/kg) (Supplementary Table 2). The average ∑LREE, ∑HREE and ∑REE concentration in saprolite was 68.81 mg/kg, 20.68 mg/kg and 89.49 mg/kg respectively (Supplementary Table 2). The ratio of $(LREE/HREE)_N$, $(La/Yb)_N$ and La/Y in bauxite and laterite varied from 0.89 to1.96, 0.67 to 2.49, and 0.88 to 3.62 respectively (Supplementary Table 2). The ratio in basalt ranged from about 0.35 to 0.81 $(LREE/HREE)_N$, 0.29 to 0.87 $(La/Yb)_N$ and 0.34 to 1.00 La/Y (Supplementary Table 2). The Eu and Ce anomalies in laterite/bauxite varied from 1.15 to 1.60 (average 1.27) and 0.97 to 2.15 (average 1.32 respectively). These anomalies in basalt ranged from 1.03 to 1.68 (Eu/Eu*) and 0.92 to 1.32 (Ce/Ce*). The chondrite-normalized $\sum(HREE)_N$ and $\sum(LREE)_N$ patterns showed a depleted nature with weathering along with high Eu and Ce anomalies (Figure 15 *a*–*e*). The saprolite sample was rich in Eu and Dy (Figure 15 *b*). For most of the samples of bauxite, laterite was characterized by a high concentration of Ce, Eu and Dy (Figure 15 *c* and *d*). Both LREE and HREE were depleted from fresh rock to bauxite/laterite, except Ce (Figure 15 *a*–*e*). The basalt and saprolite samples showed a relatively flat HREE than LREE, whereas the HREE pattern in bauxite and laterite samples was highly irregular and sharper than LREE (Figure 15 *a*–*d*). The bauxite samples mostly showed positive Ce anomalies (Ce/Ce*), which indicates the oxidizing condition during the ore-forming process[55] (Figure 15 *c*). The variation of La/Y ratio in bauxite was used to determine the change in pH during weathering[56,57] (Figure 16 *a* and *b*).

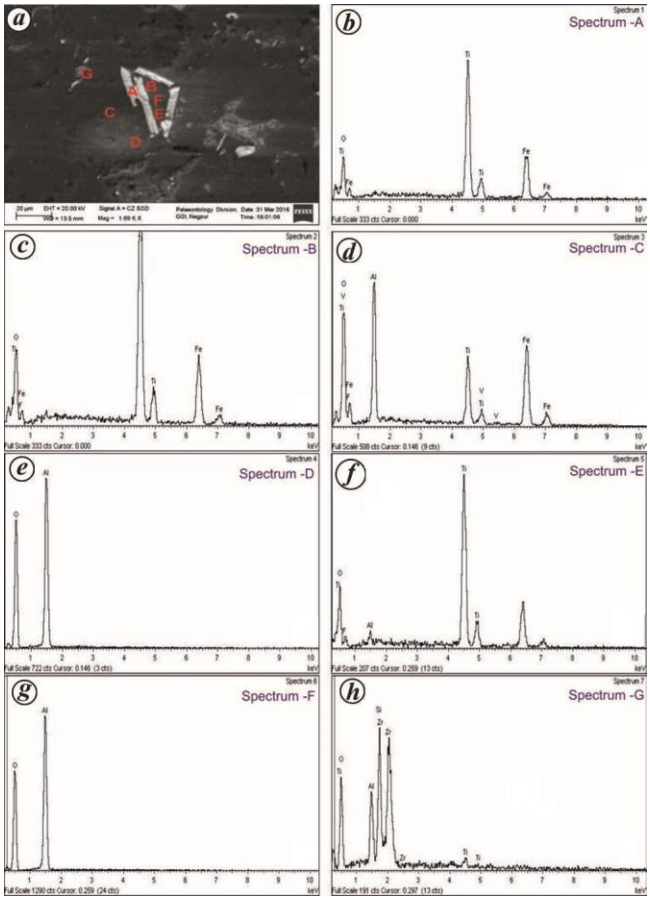

Figure 12. BSE images of bauxite ores of BH 166: Relic intergranular texture found within BH 166. Spectra A, B and E show laths of needle-shaped ilmenite grains with triangular interspaces filled by pure bauxite (spectrum F) (100 compd% Al_2O_3). Grains of ilmenite are embedded within Ti-rich bauxite (spectra C and G) or pure bauxite (spectrum D).

Discussion

The results of the present study, in terms of major and trace elements characteristics, indicate that the highly mobile and soluble constituents like Si, Mg, Ca, Na and K are leached out from basalt, while the least mobile chemical constituents like Al, Fe and Ti are retained due to solubility, sorptive phenomenon and translocation[58] (Supplementary Table 2). The Al_2O_3 concentration increases from basalt to laterite with a sharp neck point at the saprolitic part. The Fe_2O_3 content increases gradually from basalt to bauxite and further increases rapidly from bauxite to laterite. The LOI content follows almost the same trend throughout the bauxitization history. The TiO_2 content is constant during the entire process. The average variation of major oxide content and chemical composition of basalt and bauxite (Supplementary Tables 1 and 2) show that the mean SiO_2 content decreases from 44.11% (basalt) to 3.79% (bauxite). The increasing Al_2O_3 and TiO_2 content from 13.06% (basalt) to 50.15% (bauxite) and 2.47% (basalt) to 7.35% (bauxite) are due to the higher ionic potential of the quadrivalent element that tends to prefer small ionic potentials which cause almost quantitative precipitation of quadrivalent elements within bauxite[59]. The variation in concentration of Si and Al within bauxite and laterite is controlled by drainage condition[60,61].

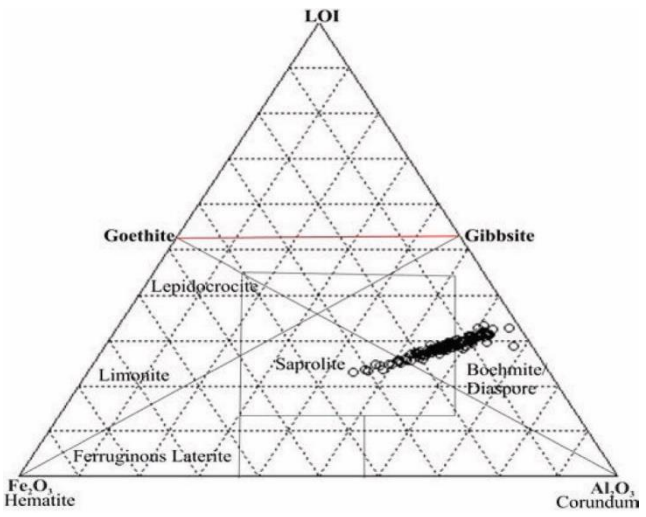

Figure 13. Ternary phase diagram of Al_2O_3–Fe_2O_3–LOI of 16 basalt, saprolite, bauxite and laterite samples[54].

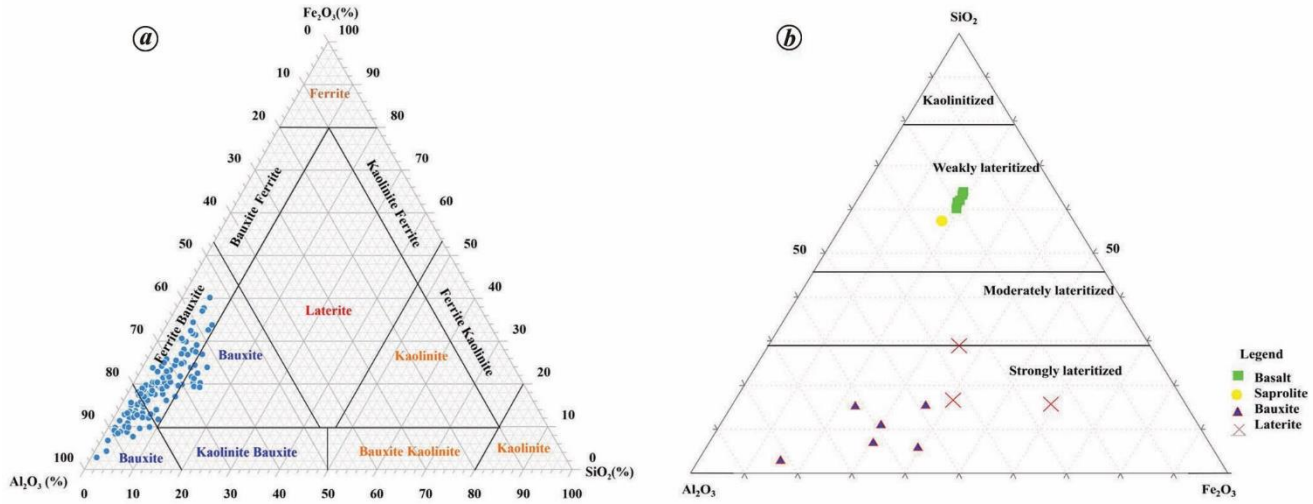

Figure 14. Fe_2O_3–Al_2O_3–SiO_2 triangular diagram showing (***a***) the mineralogical classification of 133 bauxite ores in the Bamhantara area and (***b***) degree of lateritization.

The increasing Al concentration and decreasing Si concentration within bauxite show evidence of autochthonous (or *in situ*) weathering[60,61] (Figure 4 *a*). The low amount of Si also suggests its removal during weathering in a well-drained system. The abundance of Fe from basalt to laterite suggests that iron is crystallized to form goethite and haematite as a result of intense weathering under suitable climatic conditions[62]. The uniform concentration of Ti indicates evidence of weak leaching[32] (Figure 4 *a* and Supplementary Table 2). Thus, the geochemical processes of lateritization and bauxitization occur by selective mobilization, leaching and partial re-precipitation with hydration of the elements that remain in the weathering profile.

The petrological analysis specifies that there may be two generations of boehmite present in the study area. The early-generation boehmite occurs at the core of pisolites, while the late-generation boehmite is comparatively well-crystallized and formed at the boundary of the pisolites and also in voids, pores and veinlet or incrustations (Figure 7 *a*–*d*). Gibbsite is poorly crystallized and occurs at the centre of the pisolites (Figure 7 *a*). Among the different textures, ooids and pisoids can be attributed to the heterogeneity of the initial colloids that are derived from the alteration of source rock[63]. The thin-section analysis reveals that the pisoids might have been developed from rhythmic precipitation of iron–aluminum hydroxide gel into spherical or oval bodies due to changes in the groundwater level[64] (Figures 7 *b* and 8 *a*). The process of chemical weathering is not continuous. Instead, it is formed during relatively short periods of intense weathering, separated by long periods of less intense weathering. The Bamhantara bauxitic materials were formed under oxidizing conditions as the study area was not immersed in groundwater. As the groundwater rose and submerged the area, the depositional conditions decreased. The pisolitic bauxite was formed under these conditions[64]. The pisolites are intact, circular and well-rounded in nature, which indicates the *in situ* type of depositional history[63]. The pisolitic bauxite also indicates increased drainage density in plateau bauxite[65]. Under tropical conditions, laterite may undergo desilication with the formation of concretionary bauxite[66]. The segregation of gibbsite in the form of colloform bands is due to absolute enrichment of Al or Fe resulting in the destruction of relic textures, followed by rearrangement in spherical fabrics[65] (Figure 8 *b*). It is also considered to be formed by colloidal deposition of aluminous and ferruginous material followed by recrystallization[67]. The colloidal growth may be due to the variation of rhythmic differentiation of Fe^{+3} and Al^{+3} of the hydroxyl-gel. The alumino-ferruginous material within the aggregates of fine to medium-grained gibbsite indicates the possible redistribution of Fe in the bauxite profile[47,63,68] (Figure 6 *a* and *b*). It has been observed that the core of the pisolites was mainly formed by gibbsite–boehmite transitional phase or boehmitic–bauxite. The Ti and Fe contents increased from the core towards the boundary of the pisolites and formed Fe–Ti or Ti-rich bauxite. The ilmenite grains showed a cross-cutting relationship with the grain boundary of bauxite (Figures 10 and 11). The presence of relic intergranular texture (Figure 12) within bauxite provides direct clues that it is the result of the chemical weathering product of basalt (Deccan Traps; Figure 12). The lath-shaped ilmenite grains formed triangular interspaces that were filled up later by bauxite. Good preservation of relic texture indicates porous rock with main areas of relative aluminum enrichment in plateau bauxite[65] (Figure 12). The mineralogical composition of Bamhantara bauxite reveals iron hydroxides and accessory minerals like feldspar, zircon, rutile, anatase, ilmenite and a few clay particles. These minerals are suitable for the formation of kaolinite[69]. A low amount of kaolinite was detected in the bauxite samples. The presence of kaolinite indicates indirect bauxitization[70,71] or desilication of kaolinite[47,72,73] under hot, rainy, tropical climate[63], which

can be considered the main weathering mechanism for the formation of bauxites.

The goethite and haematite in bauxite indicate that both minerals formed during weathering in highly oxygenated conditions. The dehydration process mainly converts goethite into haematite[74,75]. The occurrence of both goethite and haematite also suggests their origin as a result of weathering in an oxygenated condition without complete dehydration of goethite. The presence of both unaltered primary mineral phases and altered products suggests that the mafic minerals such as hornblende and augite, and plagioclase from the host basaltic are converted into bauxite (strong deferruginization and elimination of kaolinite) during weathering[62]. The geochemical and textural variations of bauxite in the Kabirdham rocks suggest evidence of chemical weathering of the parent rock[61,76,77].

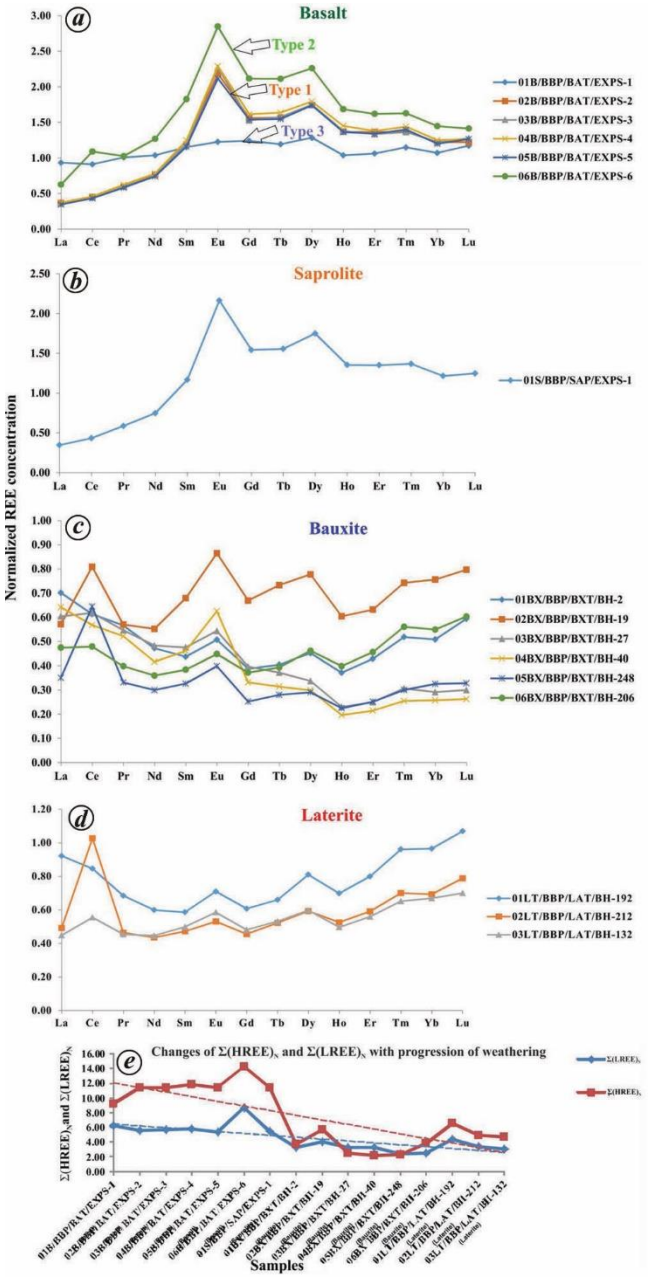

Figure 15. Chondritic normalized distribution of REE in (***a***) basalt; (***b***) saprolite; (***c***) bauxite; (***d***) laterite; (***e***) Chondrite-normalized $\sum(\text{HREE})_N$ and $\sum(\text{LREE})_N$ trend with respect to weathering.

Generally, in bauxite deposits, gibbsite, boehmite and diaspore are the predominant aluminum phases[47]. The mineralogical analysis indicates that the bauxitic mineral in the study area is boehmite with sparse occurrences of gibbsite or gibbsite–boehmite transition phase (Figure 9 *a*–*c*). The chemical composition, as shown from the triangular diagram (Fe_2O_3–Al_2O_3–LOI), also indicates that boehmite is the major mineral constituent rather than gibbsite (Figure 13 *a*). This has also been interpreted from the spectral behaviour of bauxite and laterite at Kabirdham district, Chhattisgarh[78].

The triangular plots of SiO_2, Al_2O_3 and Fe_2O_3 as the end-members drawn to classify bauxite show the degree of lateritization and reconstruct geochemical paths during bauxitization (Figures 13 *b* and 14 *a*). The figures also suggested that low amounts of kaolinite support bauxitization from basalt due to strong deferruginization and destruction of kaolinite[21,79]. Thus, the Bamhantara bauxite can be categorized into bauxite and/or ferrite–bauxite based on geochemical analysis. It indicates tropical palaeo-geographic conditions that favour bauxitization and the formation of bauxite horizons. The mineralogical changes in the parent rock led to the development of extensive lateritic bauxite deposits[62,80–82].

The trace elements concentration (Rb, Y and Nb contents) was constant during the lateralization process, except for a few elements like Zr, Ba and Sr (Supplementary Table 2). The concentration of Zr and Ba increased, and Sr content gradually decreased with weathering. The concentration of other trace elements remained constant (Figure 4 *b*).

The normalized REE distribution pattern of the weathering products mostly inherited certain geochemical characteristics of their parent materials. The Eu anomaly was considered to be retained during intense weathering and was utilized for identifying the host rock of bauxite[61,83,84]. The samples from basalt, laterite and bauxite showed positive Ce anomalies (Ce/Ce*) (0.92–2.15) (Supplementary Table 2), which indicates oxidizing environmental conditions. The geochemical characteristics identified three different types of basalt. Type 1 was characterized by positive Eu and Dy anomalies. Type 2 was identified by positive Ce, Eu and Dy anomaly and Type 3 exhibited a relatively flat REE pattern along with positive Dy anomaly and no Eu anomaly (Figure 15 *a*). Therefore, the geochemical behaviour and trend analysis of trace elements and REE suggest that saprolite was formed from type 1 under acidic conditions, while bauxite and laterite were formed from type 2 under basic conditions.

The La/Y ratio in the samples of the study area indicates the change from acidic to basic conditions with weathering (Supplementary Table 2 and Figure 16 *a*)[85,86]. La/Y < 1 implies the prevalence of acidic conditions, whereas La/Y > 1 indicates basic conditions[85,86]. As the pH of water changes gradually, silica is no more soluble in near-neutral conditions

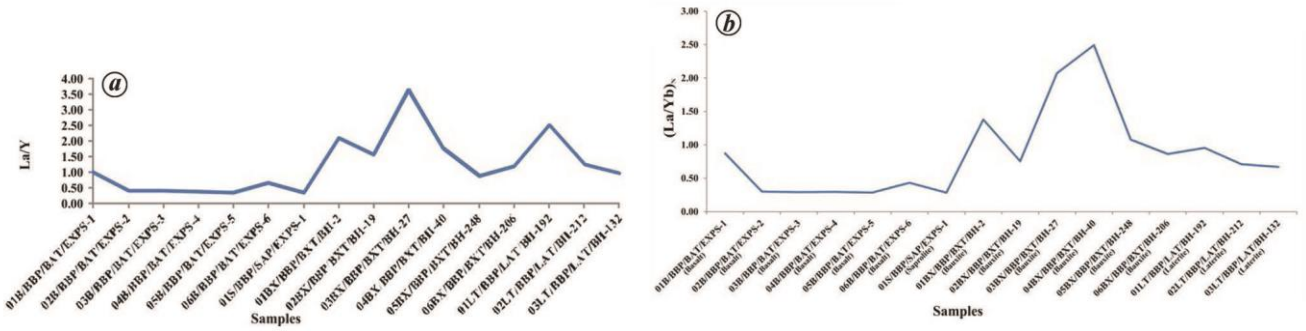

Figure 16. Changes in pH with weathering from basalt to laterite. (***a***) La/Y ratio and (***b***) $(La/Yb)_N$ ratio in samples of the study area.

than in acidic conditions[87]. The absorption of silica on Al-hydroxides leads to the formation of kaolinite in saprolite. Further desilication of saprolite and laterite ultimately leads to the formation of bauxite. The $(La/Yb)_N$ ratio in bauxite is controlled by pH fluctuations in the soil solution[88]; the lower $(La/Yb)_N$ ratio indicates more acidic conditions. The trend of $(La/Yb)_N$ ratio in the samples of the study area shows the change from acidic to basic conditions with weathering (Supplementary Table 2 and Figure 16 *b*). Therefore, the mineralogical study has a major role in the distribution of trace elements[89–91], REEs[80,92] and their behaviour in regolith profiles[68,74].

Thus, the Bamhantara bauxite forms under intense leaching in an acidic or neutral medium and an intensely oxidizing environment with a hot and moist climate[93].

Conclusion

The following conclusions can be drawn from the present study.

- The Bamhantara laterite profile consists of a complete progression from unaltered basalt bedrock through subaerial weathering developed as a result of intense substrate alteration under tropical or subtropical climates and leaching through geological time.
- The Bamhantara bauxite is a type of autochthonous (circular, well-rounded pisolites) deposit that locally experienced transportation and re-deposition under syn-environmental depositional condition (presence of boehmite).
- The bauxite layer is categorized as bauxite and/or ferrite–bauxite based on geochemical analysis.
- Bauxite had formed by desilication of kaolinite under a hot, rainy, tropical climate with an intensely oxidizing subtropical to tropical environment (presence of boehmite, gibbsite and boehmite–gibbsite transitional phase) under a high degree of drainage (presence of pisolites).
- The rhythmic precipitation of iron–aluminum hydroxide in bauxite occurred due to groundwater fluctuation (formation of pisolites).
- The presence of relic inter-granular texture and relic feldspar within bauxite provides direct clues that bauxite is the result of chemical weathering product of basalt (Deccan Traps).
- Uniform concentration of Ti indicates weak leaching.
- The same REE patterns for bauxite/laterite probably reflect a homogeneous parent rock from which the Bamhantara lateritic bauxite was derived under tropical to subtropical climates.
- The geochemical behaviour and trend analysis of trace elements and REEs revealed that saprolite was formed from type 1 basalt under acidic conditions, while bauxite and laterite from type 2 basalt under basic conditions.

Conflict of interest: The authors declare no conflict of interest.

1. Retallack, G. J., Lateritization and bauxitization events. *Econ. Geol.*, 2010, **105**, 655–667.
2. Ouyang, Y., Liu, H., Wang, X., Liu, S., Zhang, J. and Gao, H., Spatial distribution prediction of laterite–bauxite in Bolaven Plateau using GIS. *J. Earth Sci.*, 2019, **30**, 1010–1019.
3. Freyssinet, P. H., Butt, C. R. M., Morris, R. C. and Piantone, P., Ore-forming processes related to lateritic weathering. *Econ. Geol.*, 2005, **31A**(6), 547–558.
4. Roy Chowdhury, M. K., Venkatesh, V., Anandalwar, M. A. and Paul, D. K., Recent concepts on the origin of Indian laterite. Geological Survey of India, Calcutta, 1965; http://www.new.dli.ernet.in/rawdatauploud/upload/insa/INSA1/20005ab9547.pdf (accessed on 12 September 2011).
5. Bland, W. and Rolls, D., *Weathering: An Introduction to the Scientific Principles*, Arnold, London, UK, 1998, p. 271.
6. Schaetzl, R. J. and Anderson, S., *Soils: Genesis and Geomorphology*, Cambridge University Press, Cambridge, UK, 2005.
7. Tan, L. G., A summary of the formation and distribution law of gibbsite-type bauxite deposit at home and abroad. *J. Wanxi Univ.*, 1999, **15**(2), 43–46 (in Chinese with English abstract).
8. Yang, Z. Y., World bauxite reserves and distribution. *World Nonferr. Met.*, 1990, **8**, 7–11 (in Chinese with English abstract).
9. Mondillo, N., Herrington, R. and Boni, M., Bauxites. In *Reference Module in Earth Systems and Environmental Sciences, Encyclopedia of Geology (Second Edition)*, Elsevier, 2021, pp. 694–707.
10. Mahoney, J. J., Deccan traps. In *Continental Flood Basalts* (ed. Macdougall, J. D.), Kluwer, Dordrecht, The Netherlands, 1988, pp. 151–194.
11. Ramkumar, M., Menier, D., Mathew, M., Santosh, M. and Siddiqui, N. A., Early Cenozoic rapid flight enigma of the Indian subcontinent resolved: roles of topographic top loading and subcrustal erosion. *Geosci. Front.*, 2017, **8**, 15–23.

12. McFarlane, M. J., *Laterite and Landscape*, Academic Press, London, UK, 1976.
13. McFarlane, M. J., Laterites. In *Chemical Sediments and Geomorphology* (eds Goudie, A. S. and Pye, K.), Academic Press, London, UK, 1983, pp. 401–425.
14. Summerfield, M. A., *Global Geomorphology*, Harlow, Longman, 1991, p. xxii + 547.
15. Thomas, M. F., Geomorphology in the tropics. In *A Study of Weathering and Denudation in Low Latitudes*, John Wiley, Chichester, UK, 1994, p. 460.
16. Eliopoulos, D. G. and Economou-Eliopoulos, M., Geochemical and mineralogical characteristics of Fe–Ni and bauxitic–laterite deposits of Greece. *Ore Geol. Rev.*, 2000, **16**, 41–58.
17. Golightly, J. P., Nickeliferous laterite deposits. *Econ. Geol.*, 1981, **75**, 710–735.
18. Boulange, B., Bouzat, G. and Pouliquen, M., Mineralogical and geochemical characteristics of two bauxitic profiles, Fria, Guinea Republic. *Miner. Deposita*, 1996, **31**, 432–438.
19. Colin, F., Beauvais, A., Ambrosi, J. P. and Nahon, D., Les latérites en environnement tropical, source de métaux d'intérêt économique. Assises de la Recherche Française dans le Pacifique, Noumea, New Caledonia, 2004, pp. 104–107.
20. Nahon, D., *Introduction to the Petrology of Soils and Chemical Weathering*, Wiley-Interscience, New York, 1991, p. 313.
21. Tardy, Y., *Petrology of Laterites and Tropical Soils*, Balkema, Rotterdam, The Netherlands, 1997, p. 408.
22. Traore, D., Beauvais, A., Chabaux, F., Peiffert, C., Parisot, J. C., Ambrosi, J. P. and Colin, F., Chemical and physical transfers in an ultramafic rock weathering profile: Part 1. Supergene dissolution of Pt-bearing chromite. *Am. Mineral.*, 2008, **93**(1), 22–30.
23. Traore, D., Beauvais, A., Auge, T., Parisot, J. C., Colin, F. and Cathelineau, M., Chemical and physical transfers in an ultramafic rock weathering profile: Part 2. Dissolution vs accumulation of platinum-group minerals. *Am. Mineral.*, 2008, **93**(1), 31–38.
24. Nugraheni, R. D. and Sunjaya, D., Geochemical approach to reveal the genetic occurrence of gibbsite, relative to the parent rock type in lateritic bauxites. *J. Phys.: Conf. Ser. 1363 012042*, 2019, pp. 1–11.
25. Widdowson, M., Evolution of laterite in Goa. In *Natural Resources of Goa: A Geological Perspective* (eds Mascarenhas, A. and Kalavampara, G.), 2009, pp. 35–68.
26. Lacroix, A., Les laterites de Guineeet les produitsd' alteration qui leursontassocies. *Nouv. Arch. Mus. Hist., Nat.*, 1913, **V**, 255–356.
27. von Richthofen, F. F., Führer für Forschungsreisende. Berlin, Germany, 1886, pp. 464–467.
28. Holland, T. H., On the constitution, origin and dehydration of laterite. *Geol. Mag.*, 1903, **4**, 59–69.
29. Campbell, J. M., Laterite: its origin, structure and minerals. *Afines Mag*., 1917, **17**, 67–71; 120–128; 171–179; 220–229.
30. Harrison, J. B., The residual earths of British Guiana commonly termed laterite. *Geol. Mag.*, 1910, **7**, 439–452; 488–494; 553–562.
31. Simpson, E. S., Notes on laterite in Western Australia. *Geol. Mag*., 2018, **9**, 399–406.
32. Li, P. *et al.*, Influence of geomorphology and leaching on the formation of Permian bauxite in northern Guizhou Province, South China. *J. Geochem. Explor*., 2020, **210**, 106446; doi:10.1016/j.gexplo.2019.106446.
33. Rao, N. A., A report on the reconnaissance survey of the bauxite occurrences in the in Bodai–Daldali area, Rajnandgaon District, M.P. Geological Survey India, 1978.
34. Rao, N. A., The investigation of the bauxite deposits in Bodai–Daldali area (Bodai and Kesmarda blocks), Rajnandgaon District, M.P. Geological Survey India, 1979.
35. Rao, N. A., Report on the investigation of the bauxite deposits in Bodai–Daldali area (Semsata and Rabda blocks), Rajnandgaon District, M.P. Geological Survey India, 1982.
36. Abat, L. T. *et al.*, Geological, geochemical and mineralogical characteristics of REE-bearing Las Mercedes bauxite deposit, Domiican Republic. *Ore Geol. Rev.*, 2017, **89**, 114–131.
37. Putzolu, F., Papa, A. P., Mondillo, N., Boni, M., Balassone, G. and Mormone, A., Geochemical characterization of bauxite deposits from the Abruzzi mining district (Italy). *Minerals*, 2018, **8**, 298.
38. Bhukte, P. G. *et al.*, Geochemical, mineralogical and petrological characteristics of lateritic bauxite deposits formed on Deccan Trap basalt with reference to high-level and coastal (low level) deposits of Maharashtra. *J. Geol. Soc. India*, 2020, **95**, 587–598.
39. Chandra, S., Natarajan, A. and Thorat, P. K., Stratigraphy and structure in parts of Kawardha Tehsil of Rajnandgaon District and Mungeli Tehsil of Bilaspur District, Madhya Pradesh. Geological Survey India (Unpubl.), 1982.
40. Courtillot, V. M., Feraud, H., Maluski, D., Morcau, M. G. and Besse, J., Deccan flood basalts and the Cretaceous/Tertiary boundary. *Nature*, 1988, **333**, 843–846.
41. Duncan, R. A. and Pyle, D. G., Rapid eruption of the Deccan flood basalts at the Cretaceous/Tertiary boundary. *Nature*, 1988, **333**, 841–843.
42. Das, B., Khan, M. W. Y. and Dhruw, H., Trace and REE geochemistry of bauxite deposit of Darai–Daldali plateau, Kabirdham district, Chhattisgarh, India. *J. Earth Syst. Sci.*, 2020, **129**, 117.
43. Sethumadhav, M. S., Somashekar, K. N. and Vennemann, T., Genesis of gibbsite and palaeoclimatic conditions deciphered from O and H isotopes: a case study from Deccan basalt derived lateritic residuum, India. *Int. J. Earth Sci. Eng.*, 2016, **9**, 918–923.
44. Abedini, A. and Khosravi, M., Geochemical constraints on the Triassic–Jurassic Amir–Abad karst-type bauxite deposit, NW Iran. *J. Geochem. Explor*., 2020, **211**, 106489; https://doi.org/10.1016/j.explo.2020.106489.
45. Momo, M. N., Beauvais, A., Tematio, P., Ambrosi, J. P., Yemefack, M., Yerimae, B. P. K. and Yongue-Fouateu, R., Lateritic weathering of trachyte, and bauxite formation in West Cameroon: morphological and geochemical evolution. *J. Geochem. Explor*., 2019; doi:10.1016/j.explo.2019.06.006.
46. Nyamsari, D. G. and Yalcin, M. G., Statistical analysis and source rock of the Minim–Martap plateau bauxite, Cameroon. *Arab. J. Geosci*., 2017, **10**, 415.
47. Sidibe, M. and Yalcin, M. G., Petrography, mineralogy, geochemistry and genesis of the Balaya bauxite deposits in Kindia region, Maritime Guinea, West Africa. *J. Afr. Earth Sci*., 2019, **149**, 348–366.
48. Torró, L. *et al.*, Geological, geochemical and mineralogical characteristics of REE-bearing Las Mercedes bauxite deposit, Dominican Republic. *Ore Geol. Rev*., 2017, **89**, 114–131.
49. Ling, K. Y., Zhu, X. Q., Tang, H. S., Wang, Z. G., Yan, H. W., Han, T. and Chen, W. Y., Mineralogical characteristics of the karstic bauxite deposits in the Xiuwen ore belt, Central Guizhou Province, Southwest China. *Ore Geol. Rev*., 2015, **65**, 84–96.
50. Cheney, J. T. and Crowley, P. D., Introduction to the SEM/EDS or every composition tells a story. In *Teaching Mineralogy* (eds Brady, J. B., Mogk, D. W. and Perkins III, D.), Mineralogical Society of America and National Science Foundation, 2008.
51. Patel, V. N., Trivedi, R. K., Adil, S. H. and Golekar, R. B., Geochemical and mineralogical study of bauxite deposit of Mainpat Plateau, Surguja District, Central India. *Saudi Soc. Geosci.*, 2013, **7**(9), 3505–3512.
52. Balasubramaniam, K. S., Surendra, M. and Ravi Kumar, T. V., Genesis of certain bauxite profiles from India. *Chem. Geol.*, 1987, **60**, 227–235.
53. Aleva, G. J. J., Laterites: concepts, geology, morphology and chemistry. International Soil Reference and Information Centre, The Netherlands, 1994.
54. Schellmann, W., Eineneue laterite definition. *Geol. Jahrb.*, 1982, **D58**, 31–47.
55. Chen, J., Wang, Q., Zhang, Q., Carranza, E. J. M. and Wang, J., Mineralogical and geochemical investigations on the iron-rich gibbsitic bauxite in Yongjiang basin, SW China. *J. Geochem. Explor*., 2018, **188**, 413–426.
56. Crnicki, J. and Jurkovic, I., Rare earth elements in Triassic bauxites of Croatia Yugoslavia. *Travaux*, 1990, **19**, 239–248.

57. Maksimovic, Z. and Panto, G., Contribution to the geochemistry of the rare earth elements in the karst-bauxite deposits of Yugoslavia and Greece. *Geoderma*, 1991, **51**, 93–109.
58. Dennen, W. H. and Norton, H. A., Geology and geochemistry of bauxite deposits in the lower Amazon basin. *Econ. Geol*., 1977, **72**, 82–89.
59. Goldschmidt, V. M., The principle of distribution of chemical elements in minerals and rocks. *J. Chem. Soc.*, 1937, 655–673.
60. Combes, P. J. and Bárdossy, G., Geodynamics of bauxites in the Tethyan realm. In *The Tethys Ocean* (eds Nairn, A. E. M. *et al.*), Springer US, Boston, MA, USA, 1996, pp. 347–365.
61. Mameli, P., Mongelli, G., Oggiano, G. and Dinelli, E., Geological, geochemical and mineralogical features of some bauxite deposits from Nurra (Western Sardinia, Italy): insights on conditions of formation and parental affinity. *Int. J. Earth Sci.*, 2007, **96**, 887–902.
62. Singh, B. P. and Srivastava, V. K., Petrographical, mineralogical, and geochemical characteristics of the Palaeocene lateritic bauxite deposits of Kachchh Basin, Western India. *Geol. J.*, 2018, **54**, 2588–2607.
63. Gu, J., Zhilong, H., Hongpeng, F., Zhongguo, J., Zaifei, Y. and Jiawei, Z., Mineralogy, geochemistry, and genesis of lateritic bauxite deposits in the Wuchuan–Zheng'an–Daozhen area, Northern Guizhou Province, China. *J. Geochem. Explor*., 2013, **130**, 44–59.
64. Zhang, J.-Y., Wang, Q., Liu, X.-F., Zhou, G.-F., Xu, H.-P. and Zhu, Y.-G., Provenance and ore-forming process of Permian lithium-rich bauxite in Central Yunnan, SW China. *Ore Geol. Rev.*, 2022, **145**, 104862.
65. Valeton, I. (ed.), Developments in soil science. In *Bauxites*, 1972, 1st edn.
66. Harrison, J. B., The katamorphism of igneous rocks under humid tropical conditions. Imperial Bureau of Soil Science, Rothamsted Experimental Station, Harpenden, England, UK, 1933.
67. Rao, J. J. and Murthy, C. V. K., Some observation on the mineralogy and geochemistry of Hazaridadar and Raktidadar plateau, Amarkantak area, M.P., India. In Proceedings of Seminar on Latertization Processes, Oxford and IBH, New Delhi, 1982, pp. 89–103.
68. Calagari, A. A. and Abedini, A., Geochemical investigations on Permo-Triassic bauxite horizon at Kanisheeteh, east of Bukan, West Azarbaidjan, Iran. *J. Geochem. Explor.*, 2007, **94**, 1–18.
69. Hanilçi, N., Geological and geochemical evolution of the Bolkardağı bauxite deposits, Karaman, Turkey: transformation from shale to bauxite. *J. Geochem. Explor.*, 2013, **133**, 118–137.
70. Boulangé, B. and Millot, G., La distribution des bauxites sur le craton Ouest-Africain. *Sci. Géol. Bull.*, 1998, **41**(1), 113–123.
71. Tardy, Y. and Nahon, D., Geochemistry of laterites, stability of AI–goethite, AI–hematite and Fe^{3+} kaolinite in bauxites and ferricretes: an approach to the mechanism of concretion formation. *Am. J. Sci*., 1985, **285**, 865–903.
72. Lelong, F., Tardy, Y., Grandin, G., Trescases, J. J. and Boulangé, B., Pedogenesis, chemical weathering, and processes of formation of some supergene ore deposits. In *Handbook of Stratabound and Stratiform Deposits 6* (ed. Wolf, K. H.), Elsevier, New York, USA, 1976, pp. 93–173.
73. Monsel, D. A. and Bergen, M. J., Bauxite formation on Proterozoic bedrock of Suriname. *J. Geochem. Explor.*, 2017, **180**, 71–90.
74. Bárdossy, G. and Aleva, G. J. J., *Lateritic Bauxites*, Elsevier, Amsterdam, The Netherlands, 1990.
75. Meyer, F. M., Happel, U., Hausberg, J. and Wiechowski, A., The geometry and anatomy of the Los Pijiguaos bauxite deposit, Venezuela. *Ore Geol. Rev.*, 2002, **20**, 27–54.
76. Liu, X. F., Wang, Q. F., Deng, J., Zhang, Q. Z., Sun, S. L. and Meng, J. Y., Mineralogical and geochemical investigations of the Dajia Salento-type bauxite deposits, Western Guangxi, China. *J. Geochem. Explor.*, 2010, **105**(3), 137–152.
77. Liu, X. F., Wang, Q. F., Zhang, Q. Z., Yang, S. J., Zhang, Y., Liang, Y. Y. and Qing, C., Transformation from Permian to Quaternary bauxite in Southwestern South China block driven by superimposed orogeny: a case study from Sanhe ore deposit. *Ore Geol. Rev.*, 2017, **90**, 1–20; doi:10.1016/j.oregeorev.2016.12.027.
78. Sarkar, D. and Sur, P., Targeting the bauxite rich pockets from lateritic terrain utilizing ASTER data: a case study from Kabirdham district, Chhattisgarh, India. *J. Earth Syst. Sci.*, 2021, **130**, 189.
79. Beauvais, A., Palaeoclimatsetdynamique d'un paysagecuirasee du Centrafreque. Morphologie, petrologieetgeochimie. Thesis. University Poitiers, France, 1991, pp. 1–315.
80. Esmaily, D., Rahimpour Bonab, H., Esna Ashari, A. and Kananian, A., Petrography and geochemistry of the Jajarm karst bauxite ore deposit, NE Iran: implications for source rock material and ore genesis. *Turk. J. Earth Sci.*, 2010, **19**, 267–284.
81. Maclean, W. H., Bonavia, F. F. and Sanna, G., Argillite debris converted to bauxite during karst weathering: evidence from immobile element geochemistry at the Olmedo Deposit, Sardinia. *Miner. Deposita*, 1997, **32**, 607–616.
82. Mordberg, L. E., Impact of crystalline basement magmatic rock composition on the geochemistry of bauxite types. In *Geochemistry of the Earth Surface. Chemical Geology* (ed. Kump, L. R.), 1993, 107, pp. 245–249; doi:org/10.1016/0009-254(93)-90184-k.
83. Liu, X., Wang, Q., Feng, Y., Li, Z. and Cai, S., Genesis of the Guangou karstic bauxite deposit in western Henan. *Ore Geol. Rev.*, 2013, **55**, 162–175.
84. Long, Y., Chi, G., Liu, J., Jin, Z. and Dai, T., Trace and rare earth elements constraints on the sources of the Yunfeng paleo-karstic bauxite deposit in the Xiuwen–Qingzhen area, Guizhou, China. *Ore Geol. Rev.*, 2017, **91**, 1–15.
85. Yang, S., Wang, Q., Deng, J., Wang, Y., Kang, W., Liu, X. and Li, Z., Genesis of karst bauxite- bearing sequences in Baofeng, Henan (China), and the distribution of critical metals. *Ore Geol. Rev.*, 2019, **115**, 1–14.
86. Zarasvandi, A., Carranza, E. J. M. and Ellahi, S. S., Geological, geochemical, and mineralogical characteristics of the Mandan and Deh-now bauxite deposits, Zagros Fold Belt, Iran. *Ore Geol. Rev.*, 2012, **48**, 125–138.
87. Krauskopf, K. B., *Introduction of Geochemistry*, McGraw Hill, Book Co, New York, USA, 1967, p. 721.
88. Mongelli, G., Boni, M., Buccione, R. and Sinisi, R., Geochemistry of the Apulian karst bauxites (southern Italy): chemical fractionation and parental affinities. *Ore Geol. Rev*., 2014, **63**, 9–21.
89. Mordberg, L. E., Geochemistry of trace elements in Palaeozoic bauxite profiles in northern Russia. *J. Geochem. Explor.*, 1996, **57**, 187–199.
90. Mordberg, L. E. and Spratt, J., Alteration of zircons: the evidence of Zr mobility during bauxitic weathering. In Goldschmidt Conference, Toulouse, France, 1998, pp. 1021–1022.
91. Paul, D. K., Titanium in bauxite. *Indian Miner*., 1969, **23**(3), 23–28.
92. Gonzalez Lopez, J. M., Bauluz, B., Fernandez-Nieto, C. and Olite, A. Y., Factors controlling the trace element distribution in fine grained rocks: the Albian kaolinite-rich deposits of the Oliete Basin (NE Spain). *Chem. Geol.*, 2005, **214**, 1–19.
93. Keller, W. D., The origin of high-alumina clay minerals – a review. *Chem., Clays Clay Miner.*, 1963, **12**, 129–151.
94. Whitney, D. L. and Evans, B. W., Abbreviations for names of rock-forming minerals. *Am. Mineral.*, 2010, **95**(1), 185–187.

ACKNOWLEDGEMENTS. We thank the Geological Survey of India (GSI), Central Region (CR), Nagpur for support. We also thank late A. K. Saha (GSI, CR, Nagpur) and M. Sridhar (formerly at GSI, Central Headquarters) for their valuable suggestions, guidance and supervision during this study.

Received 6 December 2021; revised accepted 18 January 2023

doi: 10.18520/cs/v124/i7/827-839